

---

# Foundational Inference Models for Dynamical Systems

---

Patrick Seifner<sup>1</sup> Kostadin Cvejoski<sup>1</sup> Ramsés J. Sánchez<sup>1</sup>

## Abstract

Ordinary differential equations (ODEs) underlie dynamical systems which serve as models for a vast number of natural and social phenomena. Yet inferring the ODE that best describes a set of noisy observations on one such phenomenon can be remarkably challenging, and the models available to achieve it tend to be highly specialized and complex too. In this work we propose a novel supervised learning framework for *zero-shot inference* of ODEs from noisy data. We first generate large datasets of *one-dimensional* ODEs, by sampling distributions over the space of initial conditions, and the space of vector fields defining them. We then learn neural maps between noisy observations on the solutions of these equations, and their corresponding initial condition and vector fields. The resulting models, which we call foundational inference models (FIM), can be (i) *copied and matched* along the time dimension to increase their resolution; and (ii) *copied and composed* to build inference models of any dimensionality, without the need of any finetuning. We use FIM to model both ground-truth dynamical systems of different dimensionalities and empirical time series data *in a zero-shot fashion*, and outperform state-of-the-art models which are finetuned to these systems. Our (pretrained) FIMs are available online.

## 1. Introduction

Dynamical systems are mathematical systems that change with time according to a fixed evolution rule, and serve as representational and analytical tools for phenomena, both natural and social, which generate patterns that change over time. Very often, the recorded changes of these empirical patterns are such that they can be viewed as occurring continuously in time, and thus can be represented mathematically by systems whose evolution rule is defined through differ-

ential equations. Dynamical systems governed by ordinary differential equations (ODEs) correspond to an important subset of these models, and describe the rate of change of a single, generally vector-valued function (that is, the state of the system) as time evolves, by means of a vector field (that is, the time derivative of the function). These deceptively simple systems have had a fundamental role in our understanding of many natural processes across nearly every scientific discipline — from their very introduction and application to celestial mechanics in the late seventeenth century (Newton, 1687; Bernoulli, 1712), to their function as models of concentration changes in molecular reaction networks (Hoff, 1986); oscillations in natural populations in biology (Lotka, 1925; Volterra, 1927); the process of atmospheric convection and its chaotic features (Lorenz, 1963); and the dynamics of coherent, high energy modes within turbulent flows (Noack et al., 2003), just to name a few — and continue to be the go-to mathematical objects for representing dynamic phenomena today.

This work deals with the general problem of finding the ODE (dynamical) system that best describes a set of noisy observations on a given empirical process. The current machine learning paradigm tackles this problem by (implicitly) constraining the model to handle a single process only. Indeed, practitioners typically encode their inductive biases either into the model architecture or the training objective, but optimize the model parameters to fit a single empirical distribution. One problem with this paradigm is that inference models trained to fit a single process tend to be overly specific to its distribution, and thus can rarely be reused to infer the governing dynamics of a second one, even when both processes are assumed to be described by *e.g.* similar ODE systems. Another problem is that, to succeed, the paradigm requires (i) practitioners to have access to enough observations on the process they study, to train and test their models from scratch; and that (ii) they also have the experience and expertise to face the trials and tribulations of their intricate training procedures. Note that in our context, the inductive bias is nothing but the assumption that an ODE system underlies the observations, and two representative examples that encode this assumption into the architecture and the training objective, respectively, are neural ODEs (Chen et al., 2018) and physics-informed neural networks (Karniadakis et al., 2021).

---

<sup>1</sup>Lamarr Institute. Correspondence to: Ramsés J. Sánchez <sanchez@bit.uni-bonn.de>.

A radical departure from this paradigm took place recently — first within the natural language processing community, with the advent of large language models, and second with the introduction of neural operators — and seeks instead to encode (some of) the inductive biases of interest into the training dataset itself. In fact, large language models have been shown to perform remarkably well in zero-shot down-stream tasks, after being trained on datasets which, opposite to the standard single-task paradigm, are built to contain wildly diverse demonstrations of natural language tasks, in as many domains and contexts as possible (Radford et al., 2019; Brown et al., 2020). Similarly, neural operators are able to solve differential equations in zero-shot settings, even at unseen resolutions, after being trained on carefully constructed datasets of input functions and their images under the (fixed, differential) operator being encoded (Lu et al., 2021; Kovachki et al., 2023).

We aim to set this departure onto a more concrete program with the introduction of *Foundational Inference Models* (FIM) for dynamical systems. We define FIMs as pretrained, neural models that perform *zero-shot inference* of ODE systems, whose solution encapsulate sets of noisy observations on a given empirical process. A satisfactory FIM should be able to (I) cope with dynamic phenomena of very diverse nature, and thus capture various secular and seasonal patterns, as well as non-periodic fluctuations. It should also be able to (II) handle observations from empirical processes of different dimensionalities; (III) process any number of such observations, which might be recorded regularly in time or not, and adapt its predictions and confidence accordingly; and (IV) deal with noise signals of different kinds.

The most obvious technical challenges imposed by requirements (II) and (III) above are that one does not know a priori (that is, at the time of the FIM construction) either the process dimensionality or how frequently it will be observed. Similarly, and as regards requirement (IV) above, one does not know a priori the strength of the to-be-measured noise signal, even after one has invoked maximum entropy arguments. A naive way of dealing with these challenges would be to specify ahead a maximum number of dimensions, sequence length and noise level that the model can process, but it would necessarily constrain the model’s applicability. We face these challenges by instead incorporating the notion of *compositionality* into FIM. Indeed, one of our main observations is that, without loss of generality, one can treat the components of the ODE system *that fits a given deterministic process* as independent, and hence focus only on the inference of the one-dimensional ODEs describing each dimension separately. We will empirically show that once such a one-dimensional FIM is available, it can be used to *compose* FIMs of any dimensionality and increase their time-context (that is, their resolution) without the need of any finetuning.

How can one train a model to infer one-dimensional ODEs from noisy data *in a zero-shot setting*? Our key idea is to frame the zero-shot inference problem as a supervised learning problem, and to encode our inductive biases — *viz.* ODEs as dynamical models of 1D (possibly) irregularly-sampled data — directly into a synthetic training dataset of ODEs and their solutions. Note that this dataset encodes our beliefs about the class of dynamic phenomena we expect to encounter in practice, and therefore addresses our pending requirement (I) from above. We train FIMs to map noisy and sparse observations on the solutions of these equations to their corresponding ODEs.

In what follows we first briefly review previous work on the inference of ODE dynamical systems in Section 2, which mostly follow the classical inference paradigm. Section 3 introduces our main ideas, the data generation process encoding our assumptions, and the supervised inference algorithm. We test our methodology on a benchmark of 63 ground-truth dynamical system models, 2 real-world datasets and one large scale simulation in Section 4. Finally, Section 5 closes the paper with some concluding remarks about future work, while Section 6 comments on the main limitations of our approach.

## 2. Related work

The problem of fitting an ODE dynamical system model to noisy data has many instances and, consequently, a long history in machine learning. In some applications, the functional form of the vector field can be constructed from first principles, and only a few physically interpretable parameters need to be estimated from data. Earlier solutions to this (instance of the) problem involved iteratively and numerically solving the corresponding ODE system, for some initial condition and initial guess of the unknown parameters, and then updating the latter to maximize the likelihood of the data (Bard, 1974; Biegler et al., 1986). An alternative approach, commonly known as gradient matching, avoids solving ODEs altogether and attempts instead to interpolate the noisy observations, either via splines (Varah, 1982; Ramsay et al., 2007) or Gaussian processes (Solak et al., 2002; Macdonald et al., 2015), to compute a finite difference approximation of the vector field. Gradient matching then proceeds by optimizing the model parameters to minimize the discrepancy between this finite difference approximation and the functional vector field.

In most applications one deals instead with empirical processes for which no functional form of the vector field is a priori known; it is this instance of the problem what we shall focus on. Some early proposals were close in spirit to gradient matching and simply replaced the unknown vector field with either linear function models (De Hoon et al., 2002) or Gaussian processes (Äijö & Lähdesmäki, 2009). More

recently, researchers have abandoned data interpolations and returned to numerically solving the ODE system forward in time, while leveraging sensitivity methods (Pontryagin, 1987) and modeling the unknown vector field again with Gaussian processes (Heinonen et al., 2018) or with neural networks (Chen et al., 2018). Note that these last models encode their inductive bias into the model architecture whereas (some versions of) gradient matching encode it into the training objective. Neural ODEs have been widely employed to model many continuous-time dynamical systems in the last few years, with examples ranging from direct applications to irregularly-sampled time series data (Rubanova et al., 2019; Yildiz et al., 2019; Norcliffe et al., 2021) to parameterization and inference of master equations (Seifner & Sanchez, 2023). Despite their popularity, the training of neural ODEs is known to be a formidable hurdle which many have attempted to overcome, either through regularization (Dupont et al., 2019; Finlay et al., 2020; Choromanski et al., 2020; Pal et al., 2021) or through the learning of simpler dynamics (Zhi et al., 2022), but remains a severe limitation of the model. Perpendicular to these developments runs a large family of models that use symbolic regression to infer the unknown vector field in symbolic form. We refer the reader to La Cava et al. (2021) and Makke & Chawla (2024) for contemporary reviews thereof.

All these inference models find themselves under the umbrella of the classical paradigm, insofar as they are optimized with respect to a single empirical process. There are however two recent exceptions. Similar to our approach, Becker et al. (2023) and d’Ascoli et al. (2023) generate large datasets of ODE systems and their (noisy) solutions. Opposite to us, they generate their vector fields as symbolic expressions, which limits expressivity in favor of interpretability, and tokenise the numerical solution of the corresponding ODEs. Both works frame the problem of inferring the symbolic vector field from the ODE solution as a sequence-to-sequence problem, and leverage transformer models to perform the map. The work of Becker et al. (2023) is however limited to one dimensional ODEs, whereas that of d’Ascoli et al. (2023) is limited to six-dimensional ones. Below we shall compare our methodology to that of d’Ascoli et al. (2023).

Let us finish this section by briefly commenting on the classical alternative to foundational models, namely transfer learning, which normally involves freezing a subset of weights in a pretrained model, and finetuning a smaller subset to solve the new task. Transfer learning has been recently and successfully applied to ODE inference problems via physically-informed neural networks (Desai et al., 2022; Pellegrin et al., 2022) and neural operators (Goswami et al., 2022). Yet, transfer learning inherits the problems of the classical paradigm, *viz.* it requires additional datasets and expert knowledge.

### 3. Foundational Inference Models

In this section we introduce a novel methodology to the problem of inferring ODE systems that model sets of noisy observations on  $D$ -dimensional empirical processes, in zero-shot settings.

A system of  $D$  coupled ODEs describes the rate of change of a vector-value function (of time)  $\mathbf{x} : \mathbb{R}^+ \rightarrow \mathbb{R}^D$  as time evolves, by means of a vector field  $\mathbf{f} : \mathbb{R}^+ \times \mathbb{R}^D \rightarrow \mathbb{R}^D$ . Let us write these equations in the form

$$\dot{\mathbf{x}}(t) = \mathbf{f}(t, \mathbf{x}(t)), \text{ where } \dot{\mathbf{x}}(t) = \frac{d\mathbf{x}(t)}{dt}. \quad (1)$$

To model a  $D$ -dimensional empirical process with an ODE entails assuming that the available observations correspond to the values taken by *the solution of the ODE*, at the observation times, potentially corrupted by some noise signal of which only a few statistics are known. Now, let us recall that in order to completely specify a unique ODE solution, it is necessary to specify a set of auxiliary conditions, like the initial state (condition) of the system. Accordingly, to infer an ODE system model not only entails inferring the vector field that defines it, but also the initial condition that specifies the relevant solution.

Let us now assume that we have found an ODE system defined by a vector field  $\mathbf{f}^*$ , whose solution  $\mathbf{x}^*(t)$  with respect to the initial condition  $\mathbf{x}^*(0)$  captures the observations made on our empirical process, up to some additive noise factors. Since the dynamics are assumed to be deterministic, the process is tied up with that unique solution  $\mathbf{x}^*(t)$ . Therefore we can think of the ODE system that underlies our empirical process as defined by the vector field *evaluated on the solution* associated to that process, that is  $\mathbf{f}^*(t, \mathbf{x}^*(t))$ . Such a process-dependent vector field is now a function of time only, and its correspondent (process-dependent) ODE system is now a set of  $D$  uncoupled (that is, independent) albeit complex one-dimensional ODEs.

This simple observation indicates that one does not need to explicitly deal with systems of coupled equations; inferring one-dimensional ODEs — one per each dimension of the empirical process in question — suffices. It also suggests approaching the inference of such 1D ODEs from noisy data in a different (zero-shot) key. Indeed, if to each (component of our) empirical process there is an unknown one-dimensional function (of time only)  $f^*(t)$  that approximately captures its dynamics, one can frame the zero-shot inference problem as a supervised learning problem, in which one seeks to map the set of values  $x^*(\tau_1), \dots, x^*(\tau_l)$  taken by the ODE solution  $x^*(t)$  at some observation times  $\tau_1, \dots, \tau_l$  into both the function  $f^*(t)$  and the initial condition  $x^*(0)$  that specified  $x^*(t)$  in the first place.

Since we do not know a priori the class of empirical pro-

cesses we might encounter in practice — and hence the class of vector fields and initial conditions that explain them — we opt for (i) choosing probability distributions over them, which encode our beliefs about the family of processes we aim to model; and (ii) generating synthetic datasets by sampling from these distributions and simulating the resulting ODEs. It thus follows that a model trained to map sets of values of these solutions  $(x(\tau_1), \dots, x(\tau_l))$ , on some time grid  $(\tau_1, \dots, \tau_l)$ , to their corresponding vector field ( $f$ ) and initial condition  $(x(0))$  will *by construction perform zero-shot inference* of 1D ODEs on any sequence of empirical observations. This procedure defines our FIMs for dynamical systems.

The FIM framework consist then of two main components. First, a synthetic dataset which encodes our beliefs about the empirical phenomena we aim to model. Second, an inference model that leverages ideas from neural operators (Lu et al., 2021; Kovachki et al., 2023) to map sets of observations onto continuous functions. In what follows we shall delve into the details of these two components.

### 3.1. Synthetic data generation process

In this section we describe the synthetic data generation process, through which we encode our inductive biases and address the requirements (I), (III) and (IV) proposed in the introduction. As motivated in the previous section, the FIM training dataset should consist of a set of one-dimensional ODEs (defined through their vector field) and their solutions (obtained wrt. a given initial condition). We define all these functions on the interval  $[0, T]$  for some time horizon  $T \in \mathbb{R}^+$ . The  $j$ th instance in the dataset is given by

$$f_j \sim F(\eta_j), \quad f_j : [0, T] \rightarrow \mathbb{R}, \quad (2)$$

$$x_j(0) \sim \mathcal{N}(0, \sigma_j^2), \quad (3)$$

$$x_j(t) = x_j(0) + \int_0^t f_j(\tau) d\tau, \quad (4)$$

where  $F$  is a distribution over the space of vector fields, whose hyperparameter  $\eta_j$  is sampled, together with the variance  $\sigma_j^2$  over possible initial condition, from a fixed (meta)distribution  $P$ . Before giving any details about the distributions  $F$  and  $P$ , we note that there are yet two further assumptions we need to incorporate into the data generation process, namely our lack of knowledge about the measurement process (in other words, requirement (III)) and the noise signal (requirement (IV)). We encode the former into a distribution  $G$  over possible observations grids, and the latter into a Gaussian distribution. To wit

$$\tau_1, \dots, \tau_{L_j} \sim G(\gamma_j), \quad \tau_i \in (0, T), \quad (5)$$

$$\varepsilon_{j1}, \dots, \varepsilon_{jL_j} \sim \mathcal{N}(0, \rho_j^2), \quad (6)$$

$$y_j(\tau_i) = x_j(\tau_i) + \varepsilon_{ji}, \quad (7)$$

where the hyperparameter  $\gamma_j$  and the variance  $\rho_j^2$  over possible noise signals are sampled from the same fixed (meta)distribution  $P$ .

**Distribution over the space of vector fields.** What class of vector fields give rise to ODE solutions that capture observations on naturally occurring dynamical processes? Or, put another way, what are the most likely vector fields to be found when approximating empirical processes with ODE dynamical systems? We do not attempt to answer these questions here. Instead we take a pragmatic route and define the distribution  $F$  over vector fields either via Gaussian processes, with Radial Basis Function (RBF) kernels (Williams & Rasmussen, 1995; Vert et al., 2004), or as truncated Chebyshev expansions, whose coefficients and degree are both randomly sampled. Both alternative have different hyperparameters ( $\eta$  in our context).

On the one hand, RBF kernels depend on a single free parameter  $\eta$ , which controls the scale at which variations take place. Thus a smaller  $\eta$  results in vector fields with short-range fluctuations, whereas larger  $\eta$  produce smoother vector fields that capture broader trends. When using these kernels we define the distribution  $P$  over  $\eta$  as a Beta distribution. On the other hand, truncated Chebyshev expansions can be written as

$$f_j(t) = \sum_{m=1}^{M_j} a_m^{(j)} T_m(t), \quad (8)$$

where  $T_m(t)$  is the  $m$ th Chebyshev polynomial with real coefficient  $a_m^{(j)}$ . To generate vector fields with Eq. 8 we sample both the degree  $M_j$  and the set of coefficients  $(a_1^{(j)}, \dots, a_{M_j}^{(j)})$  from  $P$ . Intuitions says that we want high order polynomials to occur rarely, and that the scale of their coefficient should also be small. We thus choose the distribution  $P$  over the degree of the polynomial to follow a Zipf law, and that over the coefficients to follow a Gaussian distribution whose variance decreases with the polynomial order like  $\frac{1}{m}$ .

In practice, we generate a dataset half of which consists of vector fields sampled from Chebyshev expansions, while the other half consists of vector fields sampled via Gaussian processes. We refer the reader to Appendix A for details on hyperparameters and the sizes of our datasets.

**Distribution over observation grids.** The FIM dataset has an inherent, fine resolution  $\Delta t$  which is specified by the fine grid on  $[0, T]$  on which we evaluate the vector fields and the ODE solutions (that is, Eqs 2 and 4 above). We choose the observation grid to be random because we do not know a priori whether the empirical processes we aim to study were recorded regularly or irregularly in time. We also do not know the recording frequency. We thus consider both regular and irregular observation grid instances. The regular



instances are defined by their instance-dependent resolution  $\Delta\tau^j \geq \Delta t$ , where  $\Delta t$  is the finest resolution within the dataset. For concreteness, we choose  $\Delta\tau^j$  uniformly from the set  $(\Delta t, 2\Delta t, 3\Delta t, 4\Delta t)$ . The irregular instances are instead defined by sub-sampling the fine grid with a Bernoulli mask of probability  $p = \frac{1}{2}$  and  $\frac{1}{4}$ . Both subsampling procedures generate observation grids with at least  $\frac{L}{4}$  points, where  $L\Delta t = T$ . This number defines the minimum number of *context* points needed by FIM to function. Additional information is provided in Appendix A.

**Noise model.** We choose to model the noise signal with a Gaussian distribution, simply because when observing a given physical process, one typically only has access to the mean square error in those observations. According to the maximum entropy principle, a Gaussian distributions is the best guess one can make (actually, the most likely distribution) given the available information (that is, given those first two moments) (Jaynes, 2003).

### 3.2. Supervised inference models

Given a set of noisy observations  $(y_1, \tau_1), \dots, (y_l, \tau_l)$  on the ODE solution  $x(t)$  as defined in the data generation process (Eq. 7 above), our goal is to estimate both the vector field  $f(t)$  and initial condition  $x(0)$  that specified  $x(t)$ . In other words, we want to reverse the data generation process. Note that we used  $y_i$  to label  $y(\tau_i)$ . Also note that we have at our disposition the set of clean observations  $(x_1, \tau_1), \dots, (x_l, \tau_l)$  too. Let us now label the set of noisy observations with  $\mathcal{O}$ , the set of clean observations with  $\tilde{\mathcal{O}}$ , the space of vector fields with  $\mathcal{F}$  and that of initial conditions with  $\mathcal{X}_0$ . We can then split the inference procedure into two steps: (i) a denoising step that maps  $\mathcal{O}$  onto  $\tilde{\mathcal{O}}$ ; and (ii) an inference step that maps  $\tilde{\mathcal{O}}$  onto  $\mathcal{F}$  and  $\mathcal{X}_0$ .

Let us, for the time being, assume that the denoising process has already been done. Learning a neural map  $h_\theta : \tilde{\mathcal{O}} \rightarrow \mathcal{F}$  can be done in the spirit of neural operators (Lu et al., 2021; Kovachki et al., 2023). The main difference is that the input space is *not* a space of functions; rather it is the space of all possible observations on the ODE solution  $x(t)$ .

Let us use  $\phi$  and  $\psi$  to denote feedforward neural networks (FFN) and sequence processing networks, respectively, where the latter can be *e.g.* LSTM (Hochreiter & Schmidhuber, 1997) or transformer networks (Vaswani et al., 2017). Let us also denote the networks’ parameters with  $\theta$ . We define a function  $h_\theta : \tilde{\mathcal{O}} \times \mathbb{R}^+ \rightarrow \mathbb{R}$  as

$$h_\theta(t) = \phi_2(\phi_1(t, \theta), \psi_1(x_1, \tau_1, \dots, x_l, \tau_l, \theta), \theta), \quad (9)$$

where the networks  $\phi_1$  and  $\psi_1$  can be interpret as the trunk and branch nets of DeepONets (Lu et al., 2021), albeit the inputs to the latter (aka sensors) are not fixed in our case. We then define the mean and variance of a Gaussian distribution

over the values that our estimated vector field can take as

$$\hat{f}(t) = \phi_3(h(t), \theta), \quad (10)$$

$$\log \text{Var}(\hat{f})(t) = \phi_4(h(t), \theta), \quad (11)$$

the variance  $\text{Var}(\hat{f})$  can be used to estimate the confidence of the model when inferring ODE from empirical processes. Furthermore, we model the initial condition  $\hat{x}(0)$  as a Gaussian random variable, whose mean and variance are given by the composition of FFNs with  $\psi_1$ , that is

$$\mu_0 = \phi_5 \circ \psi_1(x_1, \tau_1, \dots, x_l, \tau_l, \theta), \quad (12)$$

$$\sigma_0^2 = \phi_6 \circ \psi_1(x_1, \tau_1, \dots, x_l, \tau_l, \theta). \quad (13)$$

We can then integrate the mean function  $\hat{f}(t)$  to get an estimate of the ODE solution as follows

$$\hat{x}(t) = \hat{x}(0) + \int_0^t \hat{f}(\tau) d\tau. \quad (14)$$

We refer the reader to Appendix B where we provide an alternative formulation of our neural operator (Eq. 9) in terms of the kernel framework of Kovachki et al. (2023).

**Training objective.** We train to model to maximize the log-likelihood of the values taken by the vector field on a fine target grid of  $L$  points

$$\mathcal{L}_1 = - \mathbb{E}_{f_{1:L} \sim p_{\text{data}}} \left\{ \sum_{i=1}^L \frac{(f_i - \hat{f}_i)^2}{2\text{Var}(\hat{f}_i)} + \frac{1}{2} \log(\text{Var}(\hat{f}_i)) \right\}, \quad (15)$$

and minimize the one-step-ahead reconstruction error of the integrated solution

$$\mathcal{L}_2 = \mathbb{E}_{x_{1:L} \sim p_{\text{data}}} \sum_{i=1}^L (x_i - x_{i-1} - \hat{f}_{i-1} \Delta t)^2. \quad (16)$$

Note that  $\mathcal{L}_1$  corresponds to a supervised objective, whereas  $\mathcal{L}_2$  is an unsupervised one.

**Supervised denoising model.** Our supervised learning framework allows us to treat the inference and denoising problems separately. This separation opens up the door to the *composition* of FIMs with different families of denoising models. In our experiments below we shall use the popular Savitzky–Golay filter (Savitzky & Golay, 1964). However in Appendix C, we present a supervised model which can denoise time-series data in zero-shot settings, too.

### 3.3. Compositionality of FIM

Any foundational inference model should generally fulfill requirements (II) and (III) from the Introduction. Requirement (II) can be achieved with our formulation by simply leveraging different copies (instances) of our (1D)FIMs to

Table 1. Reconstruction on ODEBench. We report the percentage (%) of predictions for which the  $R^2$  score exceeds a threshold of 0.9. Results for ODEFormer, ODEFormer-opt and PySR are extracted from (d’Ascoli et al., 2023). Our results are averaged over 10 noise and subsampling realizations.

| Model         | $\rho = 0, \sigma = 0$         | $\rho = 0, \sigma = 0.05$        | $\rho = 0.5, \sigma = 0$ | $\rho = 0.5, \sigma = 0.05$ |
|---------------|--------------------------------|----------------------------------|--------------------------|-----------------------------|
| ODEFormer-opt | 75.9                           | 55.7                             | 74.7                     | 66.6                        |
| ODEFormer     | 71.2                           | 52.2                             | 69.9                     | 60.3                        |
| PySR          | 82.3                           | 63.2                             | 77.0                     | 38.2                        |
| FIM           | $84.9 \pm 0$                   | $76.5 \pm 1.2$                   | $85.3 \pm 1.5$           | $80.2 \pm 1.7$              |
| FIM-N         | <b><math>85.7 \pm 0</math></b> | <b><math>82.1 \pm 0.9</math></b> | $82.9 \pm 1.4$           | $79.6 \pm 1.5$              |

process each component of a  $D$ -dimensional process separately. We empirically demonstrate in the sections below that we can compose high-dimensional FIMs that outperform state-of-the-art models finetuned to the target datasets.

However, there are some aspects of requirement (III) that we have not fully addressed yet. Although our FIMs can (by construction) process observations recorded both regularly and irregularly in time, they have been trained to model time series data with at most  $L$  points, and at least  $\frac{L}{4}$  points (see Section 3.1).

The upper bounds could limit the applicability of FIMs to time series with more than  $L$  points. Nevertheless, we can split such time series into successive, overlapping windows and use copies (instances) of FIMs to get local estimates  $\hat{x}(t)$ . By interpolating these estimates on the window overlaps, we can combine them to a global estimate for the whole time series. We refer to Appendix D for a detailed discussion.

## 4. Experiments

In this section we test our methodology on three different tasks which involve datasets of varying complexity, different dimensionalities, and corrupted by noise signals of very different nature. The first task consists of inferring a set of 63 ground-truth dynamical systems, four of which exhibit chaotic behaviour, and comparing against the state-of-the-art symbolic regression methods of d’Ascoli et al. (2023) and Cranmer (2023), as well as against latent ODEs (Chen et al., 2018). The second task deals with dynamical systems evolving in low-dimensional manifolds and the imputation of missing values. Specifically, we perform imputation of 20% of (i) the data from the Carnegie Mellon University mo-

tion capture database (as pre-processed by Heinonen et al. (2018)) and (ii) a Navier-Stokes simulation. Finally, we infer the hidden dynamics of the ETT (Electricity Transformer Temperature) datasets collected from electricity transformers (Zhou et al., 2021), which is widely used in forecasting tasks.

We report the results obtained from two pretrained FIMs in zero-shot settings only. We label these models FIM and FIM-N. They both need a minimum of 32 (context) points to function and differ only in that FIM-N was trained on noisy input data. Furthermore, we compose both our FIM with Savitzky-Golay filters.

### 4.1. Inferring ground-truth dynamical systems

In this first experiment we show the ability of FIMs to infer ground-truth ODE (dynamical) systems. We consider the recently introduced ODEBench dataset (d’Ascoli et al., 2023) that consists of 63 ODEs (specifically 23 1D, 28 2D, 10 3D and 2 4D equations) and their solutions, evaluated on a 512 grid. Many of these ODE systems have been used to model physical phenomena of widely different nature, and examples include the damped harmonic oscillator, the Lotka-Volterra model, the Lorentz system and the Rössler attractor — the last two exhibiting chaotic behaviour. Given some set of observations  $\{y_1, \dots, y_n\}$  on the solutions of these equations, the task consists of inferring the hidden vector field  $f(t)$  and comparing the integrated trajectory  $\hat{x}(t)$ , with the ground-truth (noiseless and dense) ODE solution  $x(t)$ . We recreate the settings in d’Ascoli et al. (2023) and consider two types of data corruption, namely (i) multiplicative noise ( $y_i = (1 + \epsilon)x_i$ ,  $\epsilon \sim \mathcal{N}(0, \sigma)$ ), and (ii) the subsampling of a fraction  $\rho$  from the observations. Furthermore, we choose  $\rho$  to be either 0 or  $\frac{1}{2}$  and  $\sigma$  to be either 0 or 0.05. We compare FIM against ODEFormer (d’Ascoli et al., 2023) and PySR (Cranmer, 2023) both of which rely on symbolic regression. Note that these models have already been shown (d’Ascoli et al., 2023) to be superior to many common symbolic regression methods (like *e.g.* SINDy), which we then do not include in our baselines. ODEFormer can be used in zero-shot mode or can be optimized to the target dataset (ODEFormer-opt). PySR is fitted to each equation separately. Details about these fitting procedures

Table 2. Reconstruction error on the Lorenz system data. Results are averaged over the 128 realizations in the test set

| Model     | MAE $\downarrow$                  | MSE $\downarrow$                  | R2 $\uparrow$                     |
|-----------|-----------------------------------|-----------------------------------|-----------------------------------|
| LatentODE | <b><math>1.93 \pm 0.69</math></b> | $9.07 \pm 7.64$                   | $0.88 \pm 0.11$                   |
| FIM       | $2.04 \pm 0.20$                   | <b><math>7.91 \pm 1.67</math></b> | <b><math>0.90 \pm 0.02</math></b> |
| FIM-N     | $2.06 \pm 0.18$                   | $8.77 \pm 1.58$                   | $0.88 \pm 0.02$                   |

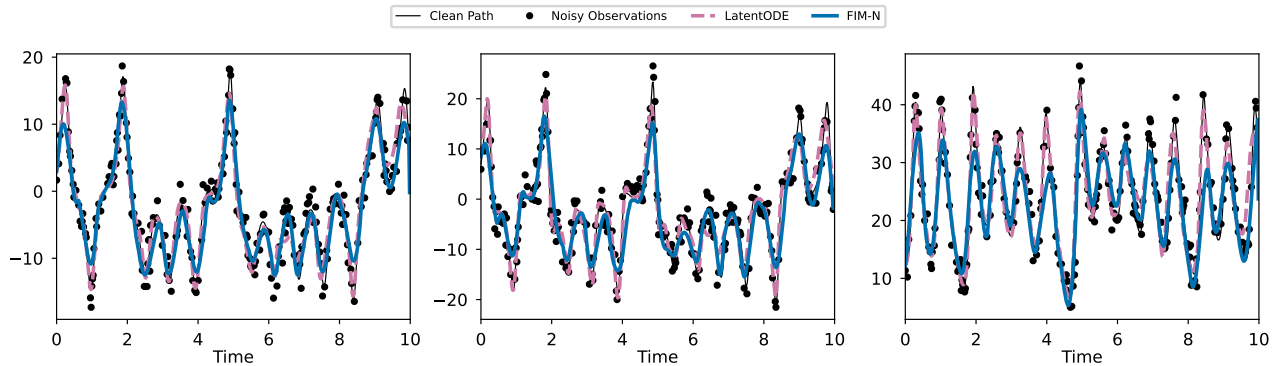


Figure 1. Inference on the Lorenz attractor time series on an irregular grid from the test set, split into their individual components. Noisy observations (black dots) of the system (black line) are interpolated by LatentODE (magenta dashed line) and FIM-N (blue line).

can be found in (d’Ascoli et al., 2023). We compose four FIM along the time axis to process the time series in all the experiments of this section.

Table 1 shows the percentage (%) of predictions for which the  $R^2$  score exceeds a threshold of 0.9, averaged over all 63 ODE solutions. Note that our models clearly outperform all baselines, even the ones that are finetuned to the data.

We now set to test FIM against a black-box ODE model which does not output a symbolic expression and hence has higher expressivity. Let us consider the Latent ODE framework of Chen et al. (2018), and apply it to the chaotic Lorenz system, as defined in ODEBench (ID 56). We simulate a set of 1280 time series, which we split into training, validation and test sets following a ratio of (8 : 1 : 1), for a set of initial conditions sampled from a Gaussian distribution with mean  $\mu = (2.3, 8.1, 12.4)$  (one of the initial conditions in ODEBench ID 56) and diagonal standard deviation  $\sigma = (1, 1, 1)$ . Again, we corrupt the data by randomly subsampling a fraction  $\rho = \frac{1}{2}$  from it, and perturbing it with a noise signal of  $\sigma = 0.05$ . Table 2 shows our (reconstruction) results with respect to the mean absolute error (MAE), mean square error (MSE) and  $R^2$  score, averaged over all 128 time series in our test set. Remarkably, both our FIMs are comparable to (and even better than) Latent ODE. Figure 1 further demonstrates the behaviour of our models when applied to an instance of the Lorenz system: Our FIMs nicely fit the ground-truth solutions.

**Ablation study.** For completeness we report in Appendix H the reconstruction errors of FIMs when applied to the ODE systems of dimensions 1, 2, 3 and 4 separately. We also report the mean absolute error (MAE), mean square error (MSE) and  $R^2$  scores (that is, not only the percentages). Specifically, Table 3 shows our results when no denoising model is applied to the input data. These results should be

compared with those in Table 4 which correspond to FIM + Savitzky–Golay configurations. The main observation we can make is that combining FIM with a denoising model significantly improves its performance in all cases (that is, in all systems, regardless of their dimension). Another interesting observation is that, besides the 3D cases which contain three out of the four chaotic systems in ODEBench, FIMs perform (in average) remarkably well (wrt. *e.g.*  $R^2$  scores) regardless of the dimensionality of the system. Figure 6 further shows the FIM reconstruction for all 63 ODE systems.

## 4.2. Low dimensional manifolds, amputations and FIM

Having demonstrated that FIMs can successfully infer ground-truth ODE systems in zero-shot settings, and even outperform models (black-box and not) finetuned on the empirical distributions under study, we would like to investigate how our methodology handles more complex, high-dimensional and experimental data. In particular we study the problem of zero-shot imputation.

One interesting application of FIM is to model systems whose dynamics mainly evolve in low-dimensional manifolds. One such case is the motion capture (MC) dataset, which consists of a 50D pose measurements from walking humans, but which is often studied as evolving in a 3D manifold (Wang et al., 2007). We use a single trajectory with 94 observations from the preprocessed dataset of Heinonen et al. (2018), and project the 50D process onto 3D space via PCA. We then remove 20% of the observations from the middle of the trajectory *in latent space* and ask FIM to recover them. FIM can perform imputation by upsampling (zero-shot super-resolution) the regions outside the gap, and then composing FIMs along time to interpolate the signal across the gap. Figure 2 displays the first three dimensions of the 50D MC trajectory, together with the

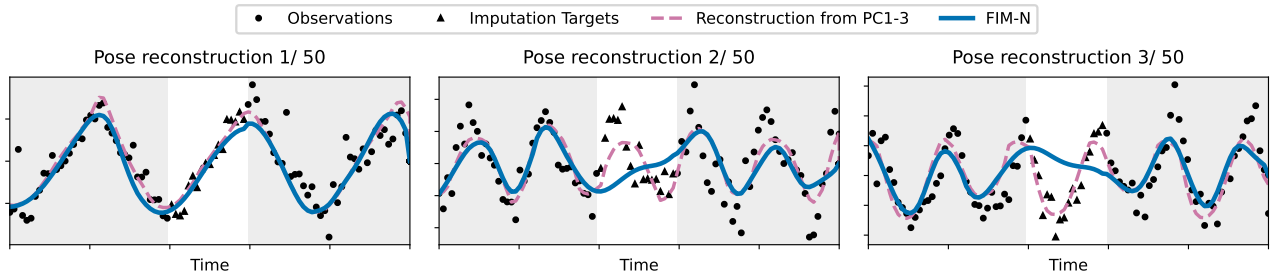


Figure 2. First 3 dimensions of the MC trajectory with imputation in data space. The trajectory is split into an observed (black dots) and an unobserved set (black triangles). Blue (Dashed magenta) lines correspond to FIM (ground-truth) reconstructions.

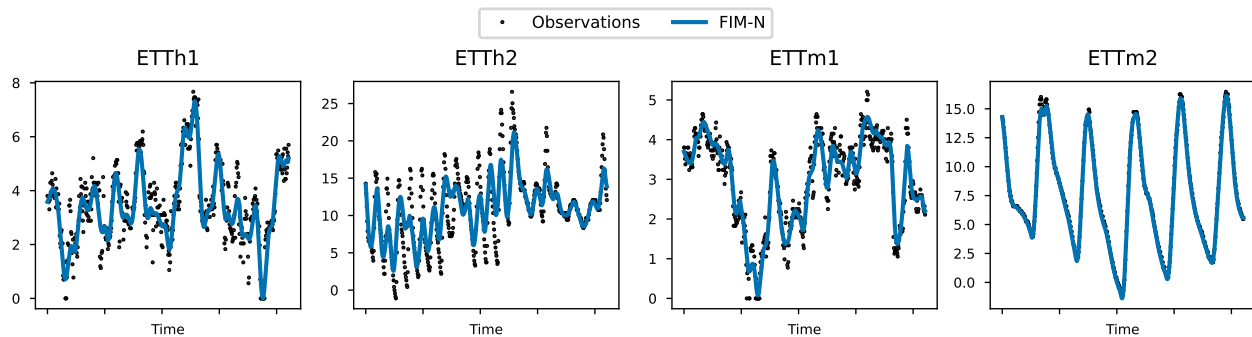


Figure 3. Zero-shot interpolation of the last component of every ETT sub-dataset with FIM-N.

reconstruction from the full 3D dynamics and the reconstruction from our imputation samples. The results show that zero-shot imputation is indeed plausible. See also Figure 5 where we additionally show the first 9 components of the 50D process. As a second experiment we also study imputations in low-dimensional manifolds of incompressible fluids past a circular cylinder (Navier-Stokes simulations) in Appendix F.

### 4.3. FIM in the wild

All experiments so far have dealt with physical systems which naturally admit a description in terms of ODEs. In this last section we consider instead noisy records of electricity consumption and show that FIM can seamlessly interpolate the data. Indeed, Figure 3 shows the last of the seven dimensions of the ETT time series dataset, together with the FIM zero-shot interpolations. Note how FIM correctly captures the fine structures and patterns in the process. Details about the ETT dataset can be found in Appendix G, and a complete study wrt. all seven dimensions of this dataset is shown in Figure 8.

## 5. Conclusions

In this work we introduced a novel methodology for zero-shot inference of dynamical systems governed by systems of ordinary differential equations. We empirically demonstrated that our foundational models successfully infer ground-truth dynamical systems of any dimensionality in zero-shot settings. We also showed that our models can perform zero-shot data imputation of complex, high-dimensional processes and seamlessly interpolate complex time series data.

## 6. Limitations

The main limitations of FIM are imposed by our synthetic dataset. Specifically by the class of vector fields and observation grids we include in it. On the one hand, inference of high frequency ODE systems is difficult for a single FIM, because of the lack of long, high frequency vector fields in our current dataset. On the other hand, FIMs require at least about 32 context points to function (already a sizeable number) regardless of the complexity of the vector field. Finding a balance between high and low frequency functions, and large and small context points within the synthetic data needs further research.



## 7. Impact statements

Our proposal could have a strong impact in the scientific community. Specifically from the point of view of accessibility to the more modern machine learning learning techniques. Indeed, foundation models do not require machine expert knowledge, which necessarily entails that they can be used by a broader community of scientist and engineers.

## References

- Äijö, T. and Lähdesmäki, H. Learning gene regulatory networks from gene expression measurements using non-parametric molecular kinetics. *Bioinformatics*, 25(22): 2937–2944, 2009.
- Bard, Y. *Nonlinear parameter estimation*. Academic Press, New York, 1974.
- Becker, S., Klein, M., Neitz, A., Parascandolo, G., and Kilbertus, N. Predicting ordinary differential equations with transformers. In *International Conference on Machine Learning*, pp. 1978–2002. PMLR, 2023.
- Bernoulli, J. Extrait de la Réponse de M. Bernoulli à M. Herman, datée de Basle le 7. Octobre 1710. (Both in *Mémoires de l’Ac. Royale des Sciences*, Boudot, Paris, 1710), 1712.
- Biegler, L. T., Damiano, J. J., and Blau, G. E. Nonlinear parameter estimation: A case study comparison. *AICHE Journal*, 32(1):29–45, 1986. doi: <https://doi.org/10.1002/aic.690320105>.
- Brown, T., Mann, B., Ryder, N., Subbiah, M., Kaplan, J. D., Dhariwal, P., Neelakantan, A., Shyam, P., Sastry, G., Askell, A., et al. Language models are few-shot learners. *Advances in neural information processing systems*, 33: 1877–1901, 2020.
- Chen, R. T., Rubanova, Y., Bettencourt, J., and Duvenaud, D. K. Neural ordinary differential equations. *Advances in neural information processing systems*, 31, 2018.
- Choromanski, K. M., Davis, J. Q., Likhoshervstov, V., Song, X., Slotine, J.-J., Varley, J., Lee, H., Weller, A., and Sindhvani, V. Ode to an ode. *Advances in Neural Information Processing Systems*, 33:3338–3350, 2020.
- Course, K. and Nair, P. B. State estimation of a physical system with unknown governing equations. *Nature*, 622 (7982):261–267, 2023.
- Cranmer, M. Interpretable machine learning for science with pysr and symbolicregression. jl. *arXiv preprint arXiv:2305.01582*, 2023.
- d’Ascoli, S., Becker, S., Mathis, A., Schwaller, P., and Kilbertus, N. Odeformer: Symbolic regression of dynamical systems with transformers. *arXiv preprint arXiv:2310.05573*, 2023.
- De Hoon, M. J., Imoto, S., Kobayashi, K., Ogasawara, N., and Miyano, S. Inferring gene regulatory networks from time-ordered gene expression data of bacillus subtilis using differential equations. In *Biocomputing 2003*, pp. 17–28. World Scientific, 2002.
- Desai, S., Mattheakis, M., Joy, H., Protopapas, P., and Roberts, S. J. One-shot transfer learning of physics-informed neural networks. In *ICML 2022 2nd AI for Science Workshop*, 2022.
- Dupont, E., Doucet, A., and Teh, Y. W. Augmented neural odes. *Advances in neural information processing systems*, 32, 2019.
- Finlay, C., Jacobsen, J.-H., Nurbekyan, L., and Oberman, A. How to train your neural ode: the world of jacobian and kinetic regularization. In *International conference on machine learning*, pp. 3154–3164. PMLR, 2020.
- Goswami, S., Kontolati, K., Shields, M. D., and Karniadakis, G. E. Deep transfer operator learning for partial differential equations under conditional shift. *Nature Machine Intelligence*, 4(12):1155–1164, 2022.
- Heinonen, M., Yildiz, C., Mannerström, H., Intosalmi, J., and Lähdesmäki, H. Learning unknown ode models with gaussian processes. In *International conference on machine learning*, pp. 1959–1968. PMLR, 2018.
- Hochreiter, S. and Schmidhuber, J. Long short-term memory. *Neural Computation*, 9(8):1735–1780, 1997.
- Hoff, J. H. v. t. *Studies in Chemical Dynamics*. Amsterdam: F. Mueller and Co. London: Williams and Norgate, 1986.
- Jaynes, E. T. *Probability Theory: the Logic of Science*. Cambridge University Press, 2003.
- Karniadakis, G. E., Kevrekidis, I. G., Lu, L., Perdikaris, P., Wang, S., and Yang, L. Physics-informed machine learning. *Nature Reviews Physics*, 3(6):422–440, 2021.
- Klambauer, G., Unterthiner, T., Mayr, A., and Hochreiter, S. Self-normalizing neural networks. *Advances in neural information processing systems*, 30, 2017.
- Kovachki, N., Li, Z., Liu, B., Azizzadenesheli, K., Bhattacharya, K., Stuart, A., and Anandkumar, A. Neural operator: Learning maps between function spaces with applications to pdes. *Journal of Machine Learning Research*, 24(89):1–97, 2023.

- La Cava, W., Orzechowski, P., Burlacu, B., de França, F. O., Virgolin, M., Jin, Y., Kommenda, M., and Moore, J. H. Contemporary symbolic regression methods and their relative performance. *arXiv preprint arXiv:2107.14351*, 2021.
- Lorenz, E. N. Deterministic nonperiodic flow. *Journal of atmospheric sciences*, 20(2):130–141, 1963.
- Loshchilov, I. and Hutter, F. Decoupled weight decay regularization. *arXiv preprint arXiv:1711.05101*, 2017.
- Lotka, A. J. *Elements of physical biology*. Williams & Wilkins, 1925.
- Lu, L., Jin, P., Pang, G., Zhang, Z., and Karniadakis, G. E. Learning nonlinear operators via deepoNet based on the universal approximation theorem of operators. *Nature machine intelligence*, 3(3):218–229, 2021.
- Macdonald, B., Higham, C., and Husmeier, D. Controversy in mechanistic modelling with gaussian processes. In Bach, F. and Blei, D. (eds.), *Proceedings of the 32nd International Conference on Machine Learning*, volume 37 of *Proceedings of Machine Learning Research*, pp. 1539–1547. PMLR, 2015.
- Makke, N. and Chawla, S. Interpretable scientific discovery with symbolic regression: a review. *Artificial Intelligence Review*, 57(1):2, 2024.
- Newton, I. *Philosophiæ Naturalis Principia Mathematica*. cf. especially Liber de Motu I Sects. II, III, VII. London, 1687.
- Noack, B. R., Afanasiev, K., MORZYŃSKI, M., Tadmor, G., and Thiele, F. A hierarchy of low-dimensional models for the transient and post-transient cylinder wake. *Journal of Fluid Mechanics*, 497:335–363, 2003.
- Norcliffe, A., Bodnar, C., Day, B., Moss, J., and Liò, P. Neural {ode} processes. In *International Conference on Learning Representations*, 2021. URL <https://openreview.net/forum?id=27acGyyI1BY>.
- Pal, A., Ma, Y., Shah, V., and Rackauckas, C. V. Opening the blackbox: Accelerating neural differential equations by regularizing internal solver heuristics. In *International Conference on Machine Learning*, pp. 8325–8335. PMLR, 2021.
- Pellegrin, R., Bullwinkel, B., Mattheakis, M., and Protopoulos, P. Transfer learning with physics-informed neural networks for efficient simulation of branched flows. *NeurIPS Workshop on Machine Learning and the Physical Sciences*, 2022.
- Pontryagin, L. S. *Mathematical theory of optimal processes*. Routledge, 1987.
- Radford, A., Wu, J., Child, R., Luan, D., Amodei, D., Sutskever, I., et al. Language models are unsupervised multitask learners. *OpenAI blog*, 1(8):9, 2019.
- Ramsay, J. O., Hooker, G., Campbell, D., and Cao, J. Parameter estimation for differential equations: a generalized smoothing approach. *Journal of the Royal Statistical Society Series B: Statistical Methodology*, 69(5):741–796, 2007.
- Rubanova, Y., Chen, T. Q., and Duvenaud, D. Latent Ordinary Differential Equations for Irregularly-Sampled Time Series. In *Advances in Neural Information Processing Systems 32*, pp. 5321–5331, 2019.
- Savitzky, A. and Golay, M. J. Smoothing and differentiation of data by simplified least squares procedures. *Analytical chemistry*, 36(8):1627–1639, 1964.
- Seifner, P. and Sanchez, R. J. Neural Markov jump processes. In *Proceedings of the 40th International Conference on Machine Learning*, volume 202. PMLR, 2023.
- Shukla, S. N. and Marlin, B. Multi-time attention networks for irregularly sampled time series. In *ICML Workshop on the Art of Learning with Missing Values (Artemiss)*, 2020.
- Solak, E., Murray-Smith, R., Leithead, W., Leith, D., and Rasmussen, C. Derivative observations in gaussian process models of dynamic systems. *Advances in neural information processing systems*, 15, 2002.
- Varah, J. M. A spline least squares method for numerical parameter estimation in differential equations. *SIAM Journal on Scientific and Statistical Computing*, 3(1):28–46, 1982.
- Vaswani, A., Shazeer, N., Parmar, N., Uszkoreit, J., Jones, L., Gomez, A. N., Kaiser, Ł., and Polosukhin, I. Attention is all you need. *Advances in neural information processing systems*, 30, 2017.
- Vert, J.-P., Tsuda, K., and Schölkopf, B. A primer on kernel methods. *Kernel methods in computational biology*, 47: 35–70, 2004.
- Volterra, V. *Variazioni e fluttuazioni del numero d’individui in specie animali conviventi*, volume 2. Società anonima tipografica” Leonardo da Vinci”, 1927.
- Wang, J. M., Fleet, D. J., and Hertzmann, A. Gaussian process dynamical models for human motion. *IEEE transactions on pattern analysis and machine intelligence*, 30(2): 283–298, 2007.
- Williams, C. and Rasmussen, C. Gaussian processes for regression. *Advances in neural information processing systems*, 8, 1995.

- Yildiz, C., Heinonen, M., and Lahdesmaki, H. Ode2vae: Deep generative second order odes with bayesian neural networks. *Advances in Neural Information Processing Systems*, 32, 2019.
- Zhi, W., Lai, T., Ott, L., Bonilla, E. V., and Ramos, F. Learning efficient and robust ordinary differential equations via invertible neural networks. In *International Conference on Machine Learning*, pp. 27060–27074. PMLR, 2022.
- Zhou, H., Zhang, S., Peng, J., Zhang, S., Li, J., Xiong, H., and Zhang, W. Informer: Beyond efficient transformer for long sequence time-series forecasting. In *Proceedings of the AAAI conference on artificial intelligence*, volume 35, pp. 11106–11115, 2021.

## A. Synthetic data generation process: Additional Information

**Sampling the space of vector fields.** The synthetic dataset that we use for training our models has in total 8M (800K for the test set) time series each containing 128 time points. Half of the time series (4M train, 400K test) are sampled from GP, where the covariance matrix is parameterized by summation of two RBF kernels ( $k_1$  and  $k_2$ ). To generate a time series  $j$ , first we sample from Beta distribution the lengthscale value ( $\eta_j^1$  and  $\eta_j^2$ ) for the two kernels. Namely, for each kernel we have two separate Beta distributions

$$\eta_j^1 \sim \mathcal{B}(2, 7), \quad (17)$$

$$\eta_j^2 \sim \mathcal{B}(5, 2). \quad (18)$$

The first kernel returns functions with faster change where as the second kernel returns smoother functions.

The second half of the dataset is contained of Chebyshev polynomials where for each time series  $j$  we sample the degree  $M_j$  from Zipf distribution (the min degree is 1 and the max degree is 100) and the coefficients of the polynomial ( $a_1^{(j)}, \dots, a_{M_j}^{(j)}$ ) are sampled from Gaussian distribution.

$$M_j \sim \text{Zipf}(2), \quad (19)$$

$$(a_1^{(j)}, \dots, a_{M_j}^{(j)}) \sim \mathcal{N}\left(0, \frac{1}{M_j}\right). \quad (20)$$

**Distribution of Observation Grids.** Each generated time series is sub-sampled to create observable data points for model input. We employ three sub-sampling schemes: full, regular, and irregular. In the *full* scheme, the entire time series is observed. For the *regular* sub-sampling scheme, observations are obtained by regularly omitted, typically every second, third, or fourth point from the fine grid. Lastly, the *irregular* sub-sampling scheme involves sub-sampling the fine grid using a Bernoulli mask with probabilities  $p = 0.5$  and  $0.25$ .

## B. Neural operator (kernel) version

Let's consider an  $M$ -layer neural operator

$$h_\theta(t) = \mathcal{P} \int k_M(t, \tau, \theta) u_M(\tau, \theta) d\tau, \quad (21)$$

where all functions  $u_i$  for  $i > 1$  are given by

$$u_{i+1}(t, \theta) = \sigma \left( w_i \cdot u_i(t) + b_i(t) + \int k_i(t, \tau, \theta) u_i(\tau, \theta) d\tau \right). \quad (22)$$

Now the function  $u_1$  has to be dealt with differently because we only have access to the input function at the observation grid  $(x_1, \tau_1), \dots, (x_l, \tau_l)$ . Thus we define

$$u_1(t, \theta) = \sigma \left( \sum_{i=1}^l k_1(t, \tau_i, \theta) \cdot (x_i \cdot w_v) \right), \quad (23)$$

with the kernel  $k_1$  defined as

$$k_1(t, \tau_i) = \frac{\exp \{ (\phi(t) \cdot w_q) \cdot (\phi(\tau_i) \cdot w_k)^T / D \}}{\sum_{n=1}^l \exp \{ (\phi(t) \cdot w_q) \cdot (\phi(\tau_n) \cdot w_k)^T / D \}}, \quad (24)$$

where the  $\phi : \mathbb{R} \rightarrow \mathbb{R}^d$  is the time embedding of Shukla & Marlin (2020), and the weights  $w_q, w_k \in \mathbb{R}^{d \times d_{\text{att}}}$  and  $w_v \in \mathbb{R}^{1 \times d_{\text{att}}}$  are learnable.



## C. Supervised denoising model

Consider

$$\hat{x}_1, \dots, \hat{x}_l, \hat{\sigma}_{x_1}, \dots, \hat{\sigma}_{x_l} = \psi_2(y_1, \tau_1, \dots, y_l, \tau_l, \theta). \quad (25)$$

with  $\psi_2$  a sequence-processing network like *e.g.* an LSTM or transformer network.

We can train this simple model to optimize the supervised loss

$$\mathcal{L}_3 = \mathbb{E}_{(x_{1:l}, \sigma) \sim p_{\text{data}}} \left\{ \sum_{i=1}^l \frac{(x_i - \hat{x}_i)^2}{2\hat{\sigma}_{x_i}^2} + \frac{1}{2} \log(2\pi\hat{\sigma}_{x_i}^2) \right\} \quad (26)$$

## D. Composing FIMs for long time series

Time series in the training set of FIMs are bounded in length by a fixed upper bound  $L$ , as described in Section 3.1. Therefore, FIMs can only (reasonably) process time series which lengths do not exceed  $L$ .

To satisfy requirement (III), adaptability of FIMs to any number of observations, we split the time series into successive, overlapping windows that are still processable by the FIMs. Applying (instances of) FIMs to each window individually yields local estimates of the solution  $\hat{x}(t)$ . To get a global estimate out of the local estimates, one can combine them on the overlaps in several way. Here we decided on a simple interpolation scheme, which is described below for two windows.

Consider two successive, overlapping time windows A and B with, associated to time windows  $[t_0^A, t_1^A]$  and  $[t_0^B, t_1^B]$  respectively. By the overlapping assumption, we have

$$t_0^A < t_0^B < t_1^A < t_1^B .$$

Applying a FIM to each window yields local solutions  $\hat{x}_A(t)$  and  $\hat{x}_B(t)$  in the respective windows. By defining

$$\hat{x}(t) = \begin{cases} \hat{x}_A(t), & \text{if } t < t_0^B \\ \frac{t_1^A - t}{t_1^A - t_0^B} \hat{x}_A(t) + \frac{t - t_0^B}{t_1^A - t_0^B} \hat{x}_B(t), & \text{if } t_0^B \leq t \leq t_1^A \\ \hat{x}_B(t), & \text{if } t > t_1^A \end{cases}$$

for  $t \in [t_0^A, t_1^B]$ , we combine  $\hat{x}_A(t)$  and  $\hat{x}_B(t)$  to a global solution  $\hat{x}(t)$  with linear interpolation on the overlap.

## E. Experimental setup

We introduce two models, denoted as FIM and FIM-N, both sharing identical architectures. The key distinction lies in their input data: the FIM model is trained using clean observations, while the FIM-N model is trained using noisy observations.

**Model Architectures:** The model contains one recurrent sub-module  $\psi_1$  and six feed-forward sub-modules  $\phi_{1-6}$ . The size of the hidden state of the model is  $h_\theta \in \mathbb{R}^{512}$ . The recurrent sub-module  $\psi_1$  which gives the input to the branch net is bi-directional LSTM with hidden size of 512. The branch net is feed-forward neural network with four hidden layers with size 1024. As trunk net  $\phi_1$ , we use the time embedding from Shukla & Marlin (2020) in combination with feed-forward neural network with 4x1024 hidden layers. The dimension of the time embedding is 512. We combine the output of the trunk net and the branch net by using feed-forward neural network  $\phi_2$  with 4 hidden layers of size 1024. The Gaussian distribution over the values that our estimated vector field is parameterized by two linear layers, one for the mean  $\phi_3$  and the second for the variance  $\phi_4$ . Lastly, for inferring the initial condition we use feed-forward neural network with 4x1024 layers. For all the feed-forward networks we use SeLU (Klambauer et al., 2017) as activation and dropout rate of 0.1.

**Hyperparameter Tuning:** For the tuning of the hyperparameters we used grid search. We used AdamW (Loshchilov & Hutter, 2017) optimizer with learning rate of  $1e^{-6}$  and weight decay  $1e^{-4}$ . The batch size is 1024.

**Training Procedure:** All the models are trained on 4 A100 80Gb GPUs. They were train approximately 500 epoch. Early stopping was used as stopping criteria. The models were trained by maximizing the likelihood. The implementation is done in Jax<sup>1</sup>. The code and trained models are provided also in the supplementary materials.

<sup>1</sup><https://jax.readthedocs.io/en/latest/index.html>

## F. Imputations and Two-Dimensional Navier-Stokes

As an application of FIMs to high-dimensional data, we consider the simulation of a two-dimensional, incompressible Navier-Stokes equation from (Course & Nair, 2023). The equation is simulated on a two-dimensional grid of size  $199 \times 1499$  for a total of 596,602 states.

For the imputation task of Figure 7, we take the test interval of Figure 3 from (Course & Nair, 2023), which consists of 40 equidistant observations in their time interval  $[256.2, 260.2]$ . We impute 8 points in the middle of the time series. The frame of Figure 7 is recorded at time 258.2, the center of the imputation window.

## G. ETT Dataset – Electricity Transformer Temperature

The ETT<sup>2</sup> from (Zhou et al., 2021) contains data of two electricity transformers, labeled 1 and 2, with two resolutions, 15 minutes (m) and 1 hour intervals (h), for a total of 4 sub-datasets. There are 7 features recorded at every observation.

For the interpolation task of Figures 3 and 8, we chose time series out of the last 20% of each sub-dataset, which is usually used as a test set for models trained on ETT data. The time series displayed are of length 512.

---

<sup>2</sup><https://github.com/zhouhaoyi/ETDataset>

## H. Additional Results

Table 3. ODEBench - Without denoising model.

| Dim | Model                                       | MAE↓          | MSE↓             | R2↑            | R2_ACC↑              | RMSE↓         |
|-----|---|---------------|------------------|----------------|----------------------|---------------|
| 1   | FIM - N                                     | 0.556 ± 0.052 | 1.808 ± 0.41     | 0.612 ± 0.245  | 0.828 ± 0.036        | 0.723 ± 0.059 |
|     | FIM   | 1.098 ± 0.141 | 6.395 ± 1.958    | -2.155 ± 3.866 | 0.691 ± 0.041        | 1.384 ± 0.178 |
|     | RBF-70-PR-NOISY                             | 0.381 ± 0.04  | 0.785 ± 0.201    | 0.583 ± 0.378  | 0.889 ± 0.03         | 0.493 ± 0.051 |
|     | RBF-70-PR                                   | 1.861 ± 0.25  | 23.099 ± 7.947   | -3.651 ± 4.65  | 0.52 ± 0.033         | 2.323 ± 0.302 |
|     | baseline                                    | 0.32 ± 0.039  | 0.559 ± 0.167    | 0.672 ± 0.237  | 0.907 ± 0.018        | 0.418 ± 0.05  |
| 2   | FIM - N                                     | 0.183 ± 0.014 | 0.297 ± 0.141    | 0.921 ± 0.024  | 0.85 ± 0.023         | 0.237 ± 0.017 |
|     | FIM   | 0.234 ± 0.028 | 0.456 ± 0.203    | 0.87 ± 0.046   | 0.845 ± 0.034        | 0.32 ± 0.037  |
| 3   | FIM - N                                     | 3.774 ± 0.19  | 76.846 ± 11.648  | 0.155 ± 0.105  | 0.185 ± 0.024        | 4.953 ± 0.242 |
|     | FIM   | 4.451 ± 0.578 | 141.019 ± 55.513 | -0.171 ± 0.227 | 0.175 ± 0.026        | 5.79 ± 0.843  |
|     | RBF-70-PR-NOISY                             | 3.631 ± 0.221 | 73.977 ± 10.079  | 0.214 ± 0.124  | 0.255 ± 0.037        | 4.817 ± 0.282 |
|     | RBF-70-PR                                   | 4.528 ± 0.214 | 106.606 ± 8.225  | -0.465 ± 0.211 | 0.135 ± 0.034        | 5.878 ± 0.233 |
|     | baseline                                    | 3.859 ± 0.301 | 88.525 ± 15.137  | 0.224 ± 0.067  | 0.28 ± 0.048         | 5.078 ± 0.349 |
| 4   | FIM - N                                     | 0.025 ± 0.003 | 0.001 ± 0.0      | 0.935 ± 0.025  | 0.875 ± 0.177        | 0.031 ± 0.003 |
|     | FIM   | 0.031 ± 0.005 | 0.002 ± 0.001    | 0.857 ± 0.064  | 0.5 ± 0.167          | 0.04 ± 0.006  |
| all | FIM - N                                     | 0.884 ± 0.034 | 12.99 ± 1.828    | 0.687 ± 0.08   | <b>0.737 ± 0.022</b> | 1.156 ± 0.045 |
|     | FIM   | 1.212 ± 0.114 | 24.921 ± 8.79    | -0.4 ± 1.417   | 0.671 ± 0.021        | 1.568 ± 0.165 |
|     | ODEFormer (opt) $\rho = 0.5, \sigma = 0.05$ | -             | -                | -              | 66.6                 | -             |
|     | ODEFormer $\rho = 0.5, \sigma = 0.05$       | -             | -                | -              | 60.3                 | -             |
|     | PySR $\rho = 0.5, \sigma = 0.05$            | -             | -                | -              | 38.2                 | -             |

Table 4. ODEBench - With Savgol filter.

| Dim | Model                                       | MAE↓          | MSE↓             | R2↑           | R2_ACC↑              | RMSE↓         |
|-----|---|---------------|------------------|---------------|----------------------|---------------|
| 1   | FIM - N                                     | 0.259 ± 0.016 | 0.341 ± 0.063    | 0.708 ± 0.088 | 0.933 ± 0.016        | 0.335 ± 0.02  |
|     | FIM   | 0.384 ± 0.034 | 0.784 ± 0.181    | 0.537 ± 0.448 | 0.926 ± 0.021        | 0.495 ± 0.04  |
| 2   | FIM - N                                     | 0.166 ± 0.018 | 0.316 ± 0.203    | 0.942 ± 0.012 | 0.871 ± 0.026        | 0.208 ± 0.023 |
|     | FIM   | 0.14 ± 0.031  | 0.222 ± 0.225    | 0.946 ± 0.025 | 0.9 ± 0.027          | 0.184 ± 0.041 |
| 3   | FIM - N                                     | 3.661 ± 0.12  | 70.72 ± 5.195    | 0.234 ± 0.087 | 0.24 ± 0.032         | 4.829 ± 0.167 |
|     | FIM   | 4.085 ± 0.532 | 111.568 ± 39.827 | 0.129 ± 0.139 | 0.215 ± 0.024        | 5.26 ± 0.725  |
| 4   | FIM - N                                     | 0.02 ± 0.002  | 0.001 ± 0.0      | 0.97 ± 0.011  | 0.95 ± 0.105         | 0.024 ± 0.003 |
|     | FIM   | 0.018 ± 0.003 | 0.001 ± 0.0      | 0.964 ± 0.022 | 0.925 ± 0.121        | 0.021 ± 0.004 |
| all | FIM - N                                     | 0.75 ± 0.022  | 11.49 ± 0.84     | 0.745 ± 0.034 | 0.796 ± 0.015        | 0.982 ± 0.029 |
|     | FIM   | 0.851 ± 0.082 | 18.094 ± 6.297   | 0.668 ± 0.17  | <b>0.802 ± 0.017</b> | 1.098 ± 0.115 |
|     | ODEFormer (opt) $\rho = 0.5, \sigma = 0.05$ | -             | -                | -             | 66.6                 | -             |
|     | ODEFormer $\rho = 0.5, \sigma = 0.05$       | -             | -                | -             | 60.3                 | -             |
|     | PySR $\rho = 0.5, \sigma = 0.05$            | -             | -                | -             | 38.2                 | -             |

Table 5. Mean and standard deviation for reconstruction metrics on a test set of the Lorenz attractor of size 128.

| Model     | MAE↓               | MSE↓               | R2↑                | RMSE↓              |
|-----------|--------------------|--------------------|--------------------|--------------------|
| LatentODE | <b>1.93 ± 0.69</b> | 9.07 ± 7.64        | 0.88 ± 0.11        | 2.83 ± 1.04        |
| FIM       | 2.04 ± 0.20        | <b>7.91 ± 1.67</b> | <b>0.90 ± 0.02</b> | <b>2.80 ± 0.29</b> |
| FIM - N   | 2.06 ± 0.18        | 8.77 ± 1.58        | 0.88 ± 0.02        | 3.00 ± 0.27        |

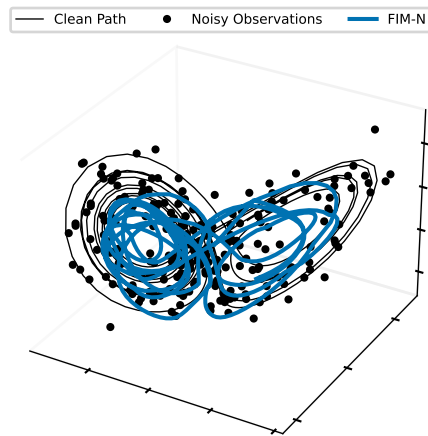


Figure 4. Inference of the Lorenz attractor time series from Figure 1 by our model. Results from our model are shown in three dimensions.

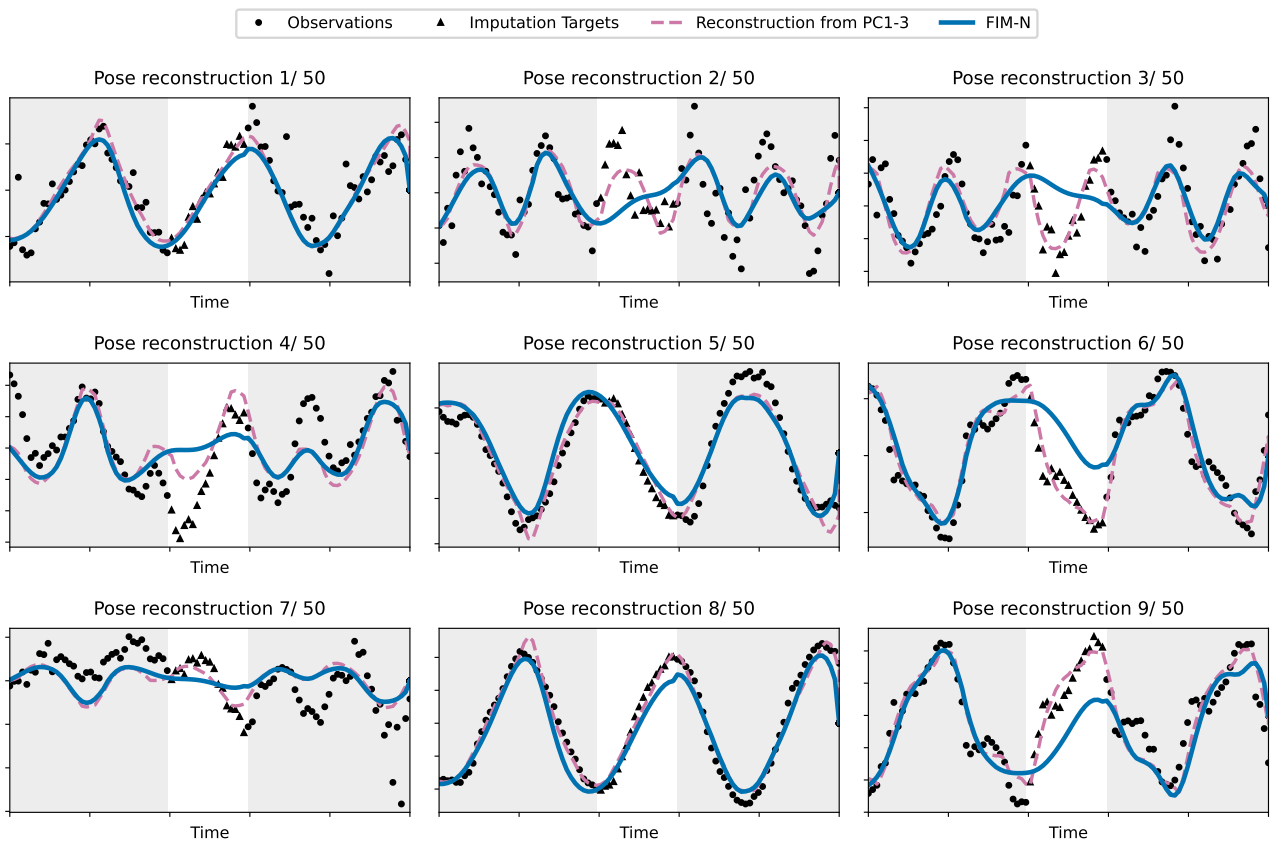


Figure 5. First 9 dimensions of a motion capture trajectory with imputation in data space. Imputation targets (black circles) are not part of the inputs (black dots). Reconstructions from our model (blue line) are based on interpolating the first 3 PCA dimensions of the trajectory. Reconstructions from the first 3 PCA dimensions of the data (magenta dashed line) are provided for comparison.



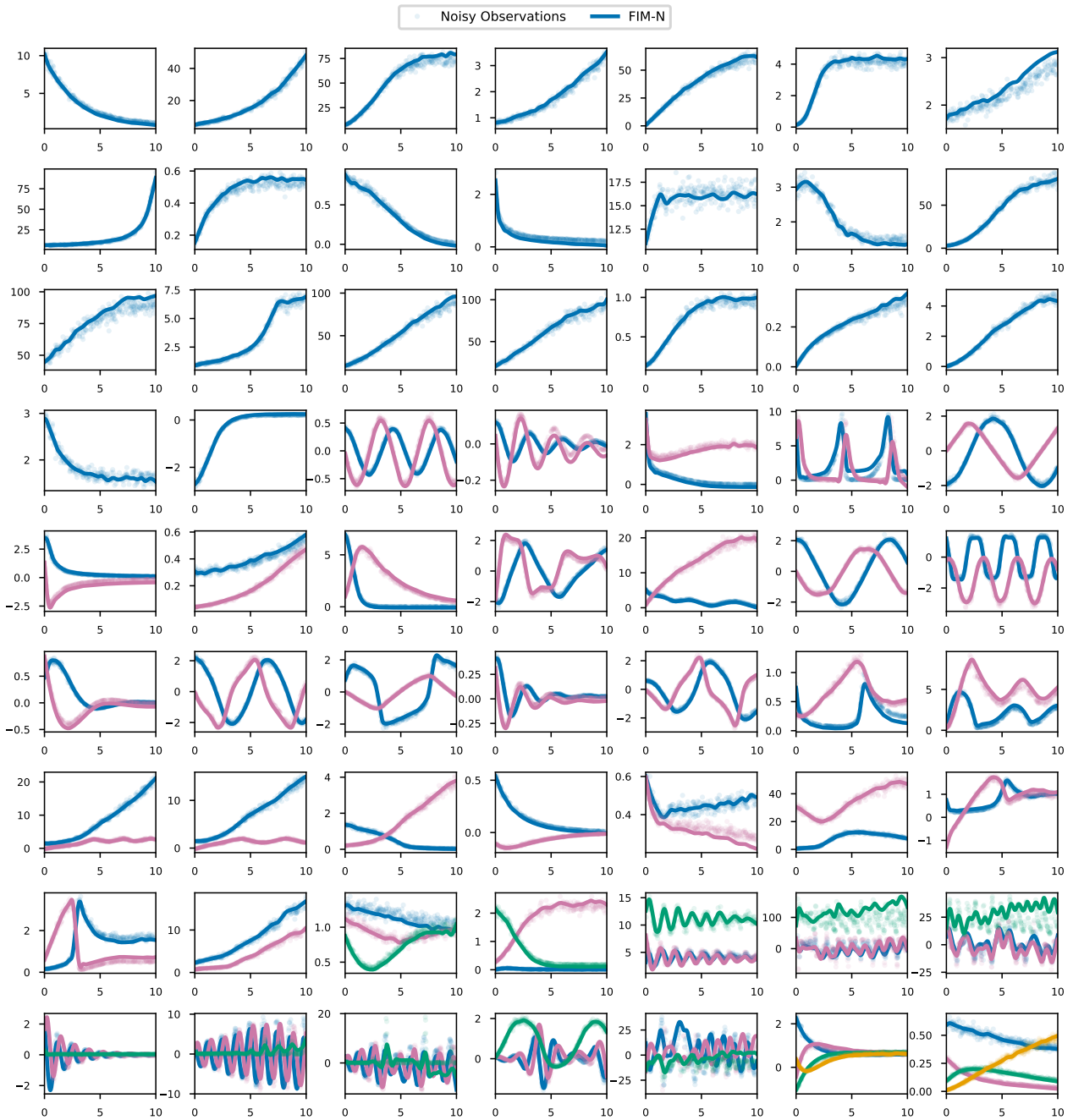
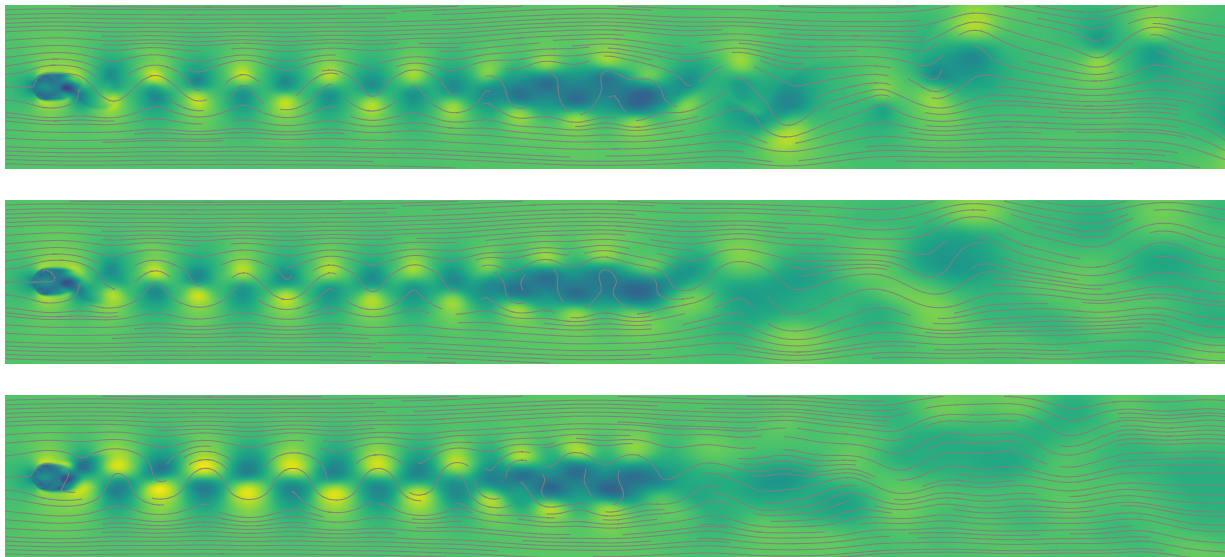


Figure 6. Reconstructions of noisy observations from of all equations in the ODEBench dataset, using the first set of initial conditions.



*Figure 7.* Imputation task on Navier Stokes trajectory test trajectory of length 40 from (Course & Nair, 2023). We drop 20% out of the center of the trajectory and impute the missing values with FIM-N. Top: observation. Mid: Reconstruction with the first 38 PCA components. Bottom: Reconstruction via imputation of FIM-N on 38 PCA components.

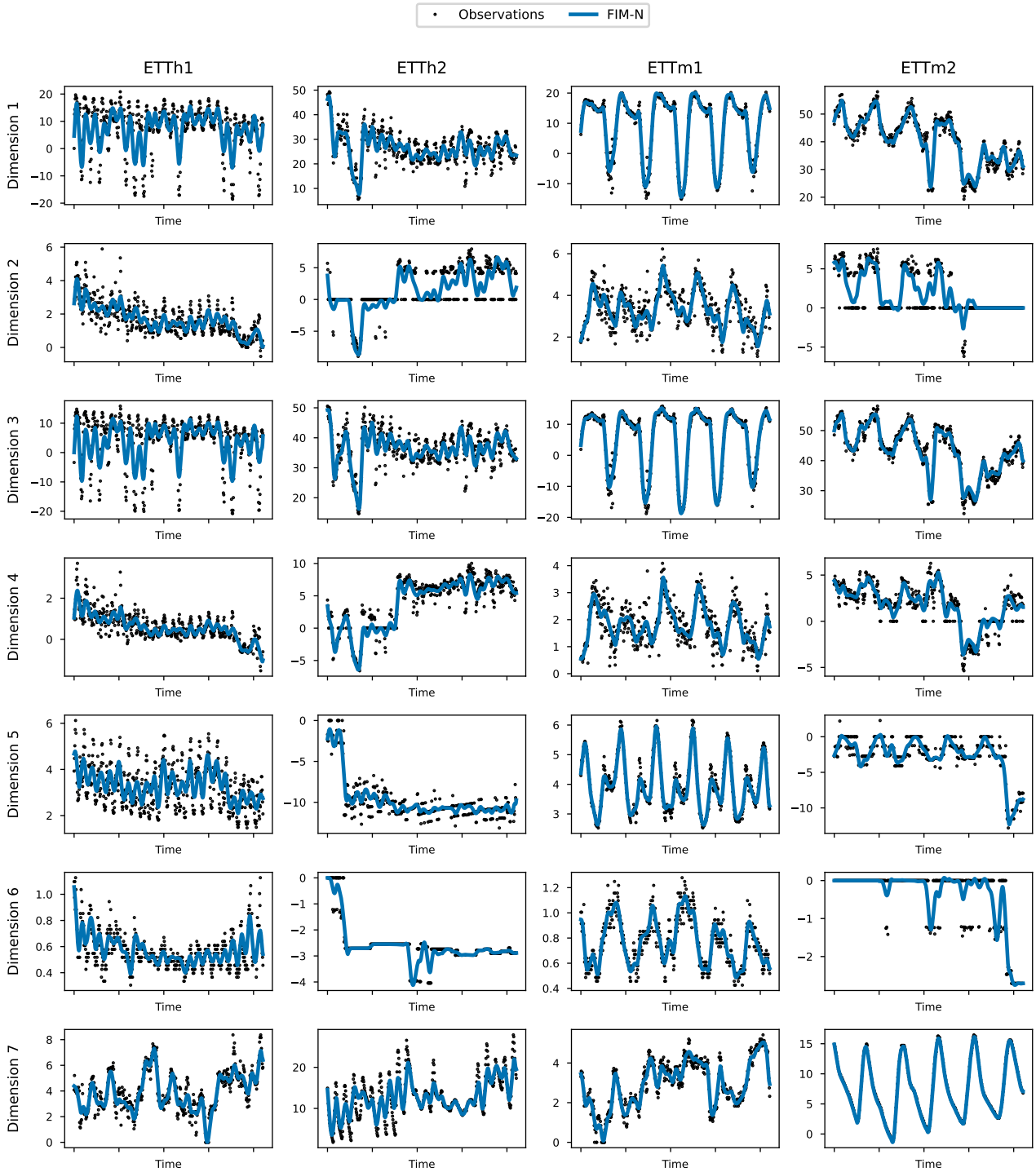


Figure 8. Interpolation of all 7 dimensions for one time series out of every ETT sub-dataset with FIM-N. The columns correspond to the sub-datasets, the rows to the individual dimensions.